JOURNAL OF MATERIALS SCIENCE 29 (1994) 4460–4476

Non-equilibrium synthesis of Fe–Cr–C–W alloy by laser cladding

J. CHOI, J. MAZUMDER
Center for Laser Aided Materials Processing, Department of Mechanical and Industrial Engineering, University of Illinois at Urbana–Champaign, Urbana IL 61801, USA

Synthesis of Fe–Cr–C–W alloy using the laser cladding technique offered an opportunity to produce a novel wear-resistant material with fine and uniform microstructure. Use of preheating during laser cladding Fe–Cr–C–W provided crack-free clads. The preheating temperature was very critical to eliminate cracks in the clad. Different complex types of carbide were observed in this research. Overall laser process parameters such as power density or specific energy as well as preheating temperature affected the characteristics of the carbide precipitates in the matrix. The increase of solid solubility and high cooling rate resulted in good metallurgical characteristics. Mostly M_6C or $M_{23}C_6$ type carbides were observed. Usually diamond-shaped M_6C carbides showed good tribological characteristics. In general, increasing the power density brought an increase of average hardness, while decreasing the power density brought a decrease of wear scar width. The laser-clad Fe–Cr–C–W alloy showed better wear properties than laser-clad Fe–Cr–Mn–C and several times smaller scar width as compared to Stellite 6 hard-facing during line-contact wear testing.

1. Introduction

Material synthesis by the laser cladding technique has recently attracted increasing attention in material processing due to the inherent rapid heating and cooling rate in laser surface modification, which provides an opportunity to produce novel materials, often overcoming the limitations related to equilibrium thermodynamics. In laser cladding and alloying processes, the surface chemistry of materials can be significantly changed by simultaneous addition of alloying elements and their subsequent rapid solidification.

Metallurgical investigations of phase transformation in Fe–Cr–C–X (X = Mn, W, V etc.) alloys have been carried out by many investigators [1–8]. A microstructural study of laser-clad Fe–Cr–Mn–C alloys revealed a high degree of grain refinement and an increase in solid solubility of alloying elements which produced a fine distribution of complex types of carbide precipitates in the ferrite matrix [3]. This study also revealed that the blocky precipitates (M_6C precipitates and χ-phase) have a higher hardness than the aligned M_7C_3-type carbide precipitates; therefore, they are expected to give rise to better wear and friction properties.

In the investigation by Eiholzer *et al.* [1] it was also reported that the wear properties of laser-clad Fe–Cr–Mn–C alloy were found to be superior to those of Stellite 6. The papers of Singh and Mazumder [2, 3] also confirmed that the laser-clad Fe–Cr–Mn–C alloys exhibited far superior wear properties compared to Stellite 6 during block-on-cylinder tests. The improved wear resistance was attributed to the fine distribution of metastable M_6C carbides.

About the alloy of Fe–Cr–C–W there is little information available in the literature. In the 1950s Goldschmidt [4] presented the first schematic diagram of Fe–Cr–C–W alloy. He reported the presence of M_6C and $Cr_{23}C_6$ carbides and also observed that $Cr_{23}C_6$ could be changed by Fe and W to form $Fe_{21}W_2C_6$ carbide. Not many types of carbide have been observed in the equilibrium Fe–Cr–C–W alloy. Recently, Uhrenius and Frondell [5] reported equilibrium associated with carbides and austenite in Fe–Cr–C–W alloy. Their study was mainly concerned with equilibrium involving $M_{23}C_6$; however, M_6C and cementite were also observed. Meanwhile, Bergstöm [6, 7] has reported the existence of M_6C carbide. The region around M_6C in the alloy was observed, and the existence of two different types of carbide, $M_{12}C$ and M_4C, was reported.

However, not much effort has been made on research about the effect of material processing parameters on Fe–Cr–C–W alloy. Recently Singh and Mazumder [9] have identified the optimum processing conditions of non-equilibrium Fe–Cr–C–W alloy. In fact, lack of understanding of the effect of processing parameters has caused many troubles during the non-equilibrium Fe–Cr–C–W laser cladding process. It should be noted that determination of suitable processing conditions have been made through many experimental trials [1–3, 9]. However, lots of things have remained unknown. Porosities between substrate and clad alloy, cracks on the clad surface as well as in the clad bulk, and keyholes in the substrate are some of the problems still not fully understood [10, 11]. These problems have to be

0022–2461

addressed before adopting the laser cladding process in the production line.

Experiments on laser-clad Fe–Cr–C–W have therefore been carried out to obtain a problem-free laser clad. Similar defects like porosities, cracking and keyholing were also observed during the laser cladding experiments. Porosities were found in many samples and did not seem to depend on the levels of power, powder feed-rate or traverse speed. One possible explanation for this may be that the substrate used, 1016 steel, contains excess gases. Upon melting of the substrate, the gases were released and became trapped in the clad due to the extremely high cooling rate. To see if this is the cause of porosity, the substrate material should be analysed for gas content to see if there is a difference between the content of those samples which exhibit porosity and those which do not. Measures could then be taken to reduce the amount of gas in the steel to reduce the occurrence of pores in the clad. The other possible explanation is that a considerably higher melting point in the clad, in this case containing Cr, W and C, than in the substrate may cause shrinkage cavities in the interface during the solidification process, because the solidification front could finish in the interface.

Many of the clads also showed extensive cracks perpendicular to the cladding direction. Some of the samples emitted audible cracking sounds immediately after the cladding process. It seems that the crack occurs due to tensile solidification stresses which result from differential expansion in the steep thermal gradients associated with laser processing. These tensile stresses usually result in cracks of the non-ductile clad layers. Two methods were considered to eliminate cracks during the processing. The first one is the reduction of carbon content in the powder with the purpose of reducing the brittleness effect during solidification. Secondly, preheated substrates were considered to reduce the severe temperature gradient change which causes the cracks. As a result, crack-free samples were obtained with the preheating method. Keyholing was also observed in some samples. It turned out to be due to excess laser power density compared to the needs of laser cladding. A proper power density is therefore, recommended to avoid the keyholing phenomenon.

Many researchers have reported wear resistance coating by laser [1, 10, 12–14]. They reported that the use of laser processing in the production of wear-resistant coatings offers considerable possibilities, giving complex microstructures with good tribological performance and strong bonds to the base metal. The laser processing technique has been used to get thin and hardened surface layers by injecting fine particles of WC or TiC into a shallow laser melt pass [10]. Eiholzer *et al.* [1] also studied the wear properties of laser-clad Fe–Cr–Mn–C. In their preliminary study, it was shown that wear resistance can be significantly improved by laser cladding to a mild steel substrate. The main motivation was to develop cobalt-free bearing alloys. However, there has been little research to replace bearing alloys with cobalt by Fe–Cr–C–W alloy, which could have better tribological properties. This will also lead to conservation of strategic elements.

The main goal of this non-equilibrium synthesis of Fe–Cr–C–W alloy was to get a fine and uniform distribution of a complex mixture of different carbide precipitate in a ferrite matrix, and to develop a crack-free clad in order to develop a cobalt-free alloy with improved tribological properties [15]. The relationships between the process parameters, carbide morphology, and wear properties were studied to evaluate the role of process parameters on the tribological properties of these non-equilibrium alloys.

2. Experimental procedure

2.1. Experimental set-up

Elemental powders of various sizes were mixed to get a mixed powder in a desirable condition. Table I shows the size and purity of the element powders. The powders were dried by heating at 200 °C in a tube furnace with a steady argon gas flow for about 8 h, and then cooled slowly to room temperature.

The experimental set-up for laser cladding (Fig. 1) consists of three units: the laser, powder dispenser and preheating furnace working simultaneously. The laser system, an Avco HPL 10 kW c.w. CO_2 laser with F7 Cassegrain optics, produces a beam with **TEM01*** mode which is doughnut-shaped with a Gaussian power distribution in the annulus.

The powder delivery system delivers powder to the substrate. It consists of an Accu-Rate (Moksness Manufacturing Inc., Whitewater, Wisconsin) powder dispenser, funnel and helium gas inlet. The powder dispenser is a screw feed system with a feed rate which was varied between 0.1342 and 1.3403 $g\,s^{-1}$. Powder falls from the screw into a funnel and flows to the small amount of helium gas flows in the tube along the powder flow for the purpose of uniformity of powder flow. This direct placement of powder for cladding into the molten pool is known to have benefits over the preplaced cladding procedure and it gives the optimum specific energy needed for cladding, resulting in a finer microstructure [16]. Helium gas was used for shielding during laser processing, because the helium has a higher ionization potential (24.6 eV) compared to argon (14.6 eV) and thus produces a plasma with a lower electron density at the laser–substrate interaction point. Loss of laser energy due to inverse Bremsstrahlung absorption at the plasma column increases with an increase of electron density.

In order to eliminate cracking due to the rapid solidification process, the preheating furnace was provided with a thermocouple and Variac which could control the temperature. The operating temperature

TABLE I Size and purity of the element powders

Element	Size (μm)	Purity (%)	wt (%)	at (%)
Fe	6–9	99.9	62.5	51.9
Cr	2	99.5	25.0	22.3
C	0–300 mesh	99.5	6.25	24.2
W	0.5	99.9	6.25	1.60

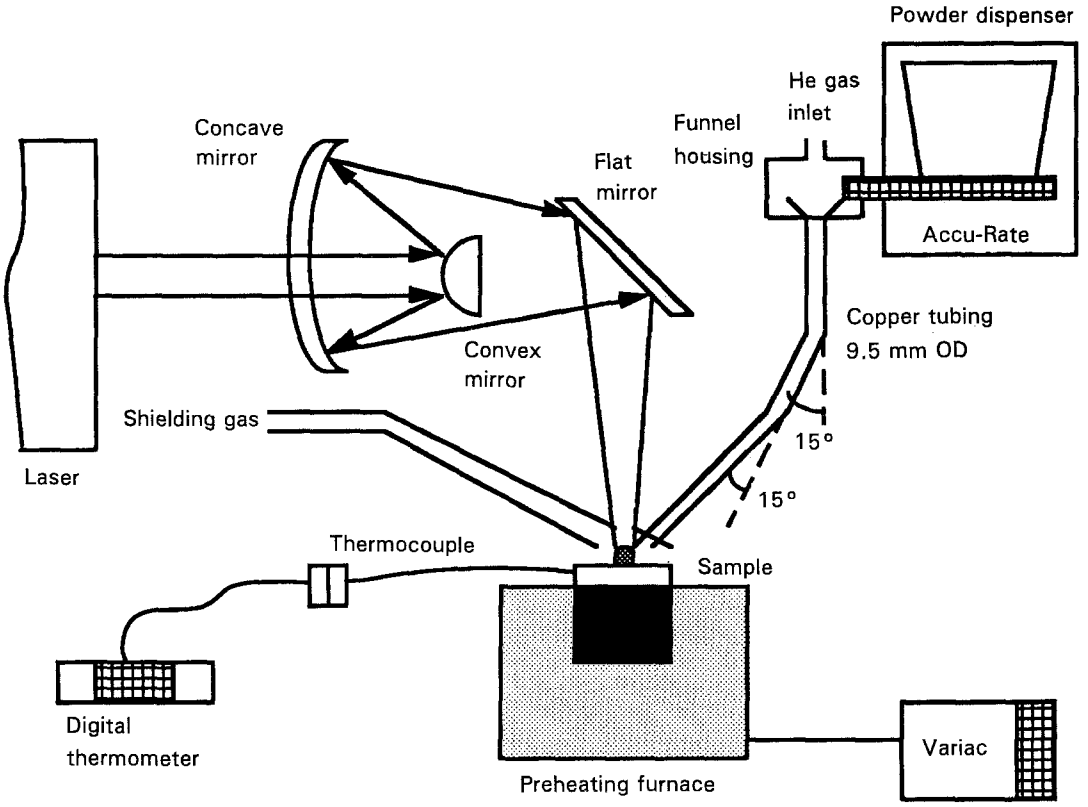

Figure 1 Experimental set-up for laster cladding.

was varied between 200 and 800 °C. The sample temperature was measured with a thermocouple.

2.2. Processing parameters and analysis procedures

The process parameters which were used for this investigation are given in Table II. For the present investigation the laser was operated at 3 to 8 kW with 2 to 4 mm beam diameter underfocused, which gives the doughnut-shaped model TEM01*. The traverse speed for the substrate was varied from 10.58 to 25.04 mm s^{-1} and the powder feed-rate was selected from 0.3142 to 1.3403 g s^{-1}. The substrate material was 0.25 in (6.4 mm) thick AISI 1016 steel with a polished surface.

For optical microscope observation, an etchant composed of 5 g $FeCl_3$, 5 g $CuCl_2$, 100 ml HCl and 300 ml H_2O was used.

A microhardness test was carried out with the Buehler model Micromet II microhardness tester to obtain the hardness distribution data. 300 g loads were applied during 7–8 s for this test with a Vickers indenter to obtain (H_V). The microhardness test data were taken from two or three different points of the same level of cross-section from the top of the surface to the interface.

TABLE II Laser process parameters

Parameter	Operating range
Laser power (kW)	3–8
Beam diameter (mm)	2–4, underfocused
Traverse speed (mm s^{-1})	10.58–25.04
Powder feed-rate (g s^{-1})	0.1342–1.3403

Microstructural and composition characterization of the clad material was performed using optical microscopy, scanning electron microscopy (SEM) (Jeol 35C, Hitachi S-800), Auger electron spectroscopy (AES) and an energy-dispersive X-ray microanalysis (EDX) system with SEM.

The cross-section of the clad area was examined using the Perkin-Elmer model PHI 660 Auger multiprobe. The cross-sections of the clad were scanned both before and after approximately 40 min of sputtering with Ar ions at 20 kV. As the amplitude of the counting peak, obtained from the AES survey, for a characteristic electron energy is proportional to the concentration of the corresponding element, the relative amounts of different elements are obtained by dividing the amplitude by the sensitivity factor. Elemental maps for AES were also obtained to understand the distribution of each element used.

Differential thermal analysis (DTA) was also carried out in order to reveal the transition temperature at the clad area for a sample without preheating. The DTA was performed with a Perkin-Elmer system 417 with a high-temperature cell attachment. Small pieces of the clad material with approximately 30 mg weight are put into a sample cup, which is filled up with Al_2O_3. The reference cup is filled up with the same level of Al_2O_3. The heating scan rate was 20 °C min^{-1} and the flow rate of Ar gas about 45 $cm^3 min^{-1}$.

A preliminary friction and wear test was performed with a block-on-cylinder machine (Fig. 2). Before the wear test, a calibration was done with a multimeter and a chart recorder by applying a load which was known, and then a chart was made. The test was

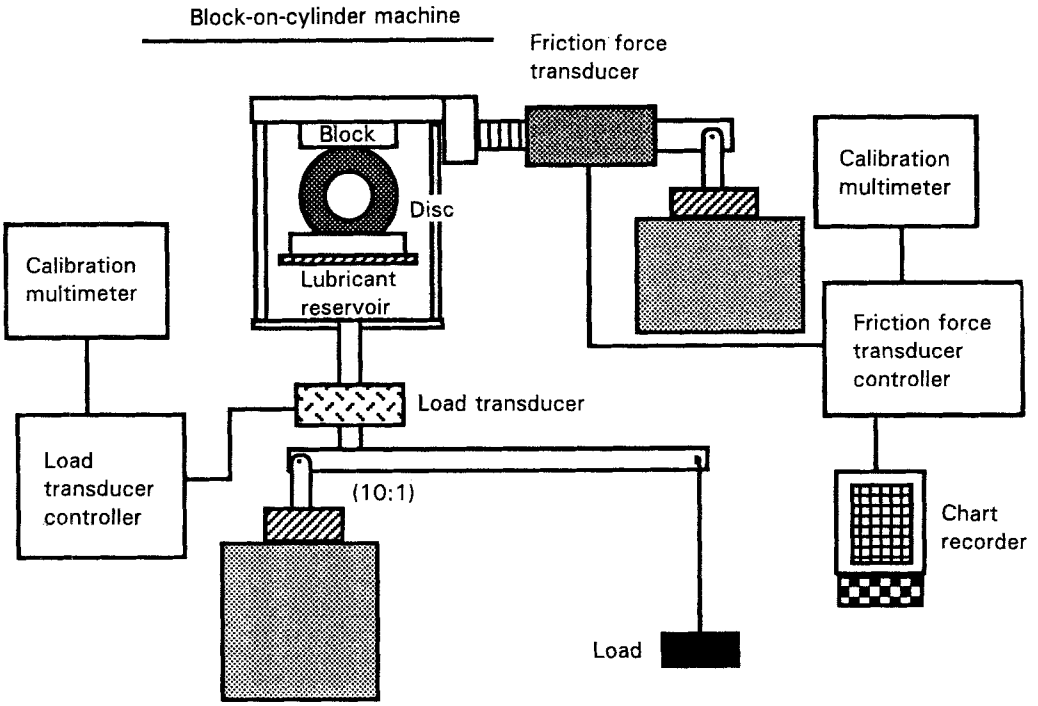

Figure 2 Schematic drawing for wear test.

monitored by measuring the voltage change by the multimeter under the load given. The load was gain-controlled by a load transducer controller. Similarly, the friction force was calculated by measuring the voltage change with a multimeter and a friction force transducer controller. The load applied on the lever was proportional to the actual test load at the block-on-ring contact by 10 : 1, i.e. 1 lb applied on the lever is equivalent to 10 lbs actual test load. The disc used for the test was AISI 52100 steel with R_c hardness 60. A wear test for which speed was set at 24 r.p.m. (0.032 m s^{-1}) was performed for 1 h per sample under boundary lubrication conditions. The lubricant used was a straight paraffinic mineral oil, Sunvice 21. During the operation, temperature and humidity were checked and controlled.

Table III shows a sample data set for the laser cladding of Fe–Cr–C–W with preheating. The samples were mainly obtained with 4 mm beam diameter, 4 kW laser power, 25 (635 mm min^{-1}) ipm traverse speed and 0.5368 g s^{-1} powder feed-rate. The laser processing parameters were varied to produce desirable data for research purposes. Power density and interaction time as well as preheating temperature were primarily considered to set up a matrix chart to understand the effect of the combination of processing parameters on the laser cladding in terms of surface condition and microstructure.

TABLE III Data set for the synthesis of Fe–Cr–C–W system (preheated)

Sample No.	Beam dia. (mm)	Laser power (kW)	Traverse speed (ipm)[a]	Powder feed-rate (gm s^{-1})	Preheat temp[b] (°C)	Specific energy (kJ cm^{-2})	Power density (kW cm^{-2})	Interaction time (s)
1-1	4	3	22	0.5368	600–621	8.05	18.75	0.4295
1-2	4	4	23	0.5368	618–667	10.27	25	0.4108
2-1	4	5	28	0.5368	612–646	10.546	31.25	0.3375
3-1	4	4	47	0.5368	586–591	5.025	25	0.201
3-2	4	4	51	0.8052	590–613	4.6325	25	0.1853
3-3	4	4	43	1.0736	590–678	5.4925	25	0.2197
7-1	4	4	23	0.5368	663–699	10.27	25	0.4108
7-2	4	4	25	0.5368	698–748	9.4475	25	0.3779
7-3	4	4	25	0.5368	725–812	9.4475	25	0.3779
8-1	3	3	26	0.5368	688–702	8.9958	33	0.2726
8-2	3	4	28	0.5368	700–735	12.376	44.4	0.2531
13-1	3	3	27	0.5368	426–454	8.6625	33	0.2625
16-1	4	4	25	0.5368	298–351	9.4475	25	0.3779
17-2	4	4	25	0.5368	384–457	9.4475	25	0.3779
19-1	4	4	25	0.5368	484–527	9.4475	25	0.3779
19-3	4	4	26	0.5368	513–652	9.085	25	0.3634

[a] 1 ipm = 25.4 mm min^{-1}.
[b] The temperature data indicate the initial steady-state temperature and the final peak temperature of the substrate during the laser processing.

3. Results

3.1. Microstructure

3.1.1. Optical microscopy and scanning electron microscopy

Microstructures of the laser-clad Fe–Cr–C–W were investigated with both optical microscopes and scanning electron microscopes. After preheating, crack-free samples were usually obtained. The preheating temperature has a very significant influence on cracking. It was found that most of the samples preheated to over 550 °C were crack-free. The overall microstructures of the laser cladding area were generally found to be uniform throughout. An optical micrograph of the laser-clad region for sample 2-1 is shown in Fig. 3. The microstructure near the interface region is, in general, a little different from that near the surface. Singh and Mazumder [3] have explained this kind of microstructure phenomenon on the basis of a heat- and mass-transfer model proposed by Li and Mazumder [16] in the case of samples without preheating.

However, in this case a consideration of preheating effect should be added to understand this phenomena, which could be explained by the rapid solidification process producing a non-equilibrium phase and the latent heat energy needed to melt the substrate near the interface during solidification. The preheating temperature would affect the differential cooling rate in the steep thermal gradient associated with laser processing, and in some sense contribute an additional layer of substrate near the interface area to melt with the latent heat energy. However, it should be noted that, during the solidification, although a preheated substrate could not permit enough time to remix and diffuse the alloying element with the remaining melt, it would allow the clad near the interface area to form a rich but uniform alloying structure–generally of higher metal concentration relative to carbide concentration (M_3C_2 or M_2C instead of M_6C or $M_{23}C_6$) – which was investigated in the AES survey. More detailed analysis may be necessary to understand the effect of preheating on the formation of duplex phases which have been observed in other laser-clad alloys such as Fe–Cr–C–Mn, Mg–Al and Ni-based alloys [3]. It was also found through AES analysis that the interface region usually had higher alloying element concentrations (about 5–10% higher when alloying with Fe, Cr and W) than the region above the interface through AES analysis.

Several types of carbide were also found such as diamond-shaped (Fig. 4a), unfaceted-block diamond type (Fig. 4b), acicular type (Fig. 4c), and cellular dendrite type (Fig. 4d). The formation of these types of carbide strongly seemed to be a function of the preheating temperature as well as the laser processing parameters. Because of the sparse information on the phase diagram of Fe–Cr–C–W alloys it was difficult to judge what the transition temperature for the phase change was. The transition temperature would be involved in causing the transformation of different carbides.

3.1.2. Differential thermal analysis

DTA was carried out in order to obtain transition temperature information. A sample without preheating was examined as shown in Fig. 5. This indicates that the transition temperature could be between 590 and 610 °C. Although this temperature may be only one of the transition temperatures for this particular alloy, such information could give some ideas for predicting the preheating effect.

Fig. 6a and b compare the microstructures before and after DTA. This shows that the size of carbide precipitates significantly increases after DTA. The size of precipitates before DTA was about 2–3 μm but after DTA was about 8–10 μm. The heating and cooling process during DTA results in annealing of the microstructure. The microstructure before DTA shows sharp and random-directional phases due to the extremely high cooling rate, while the microstructure phases after DTA were not so sharp compared to those before DTA.

3.1.3. SEM energy-dispersive X-ray analysis

Initially SEM EDX analysis was performed in order to obtain volume fraction information for the carbides. Just a little information about the carbides was

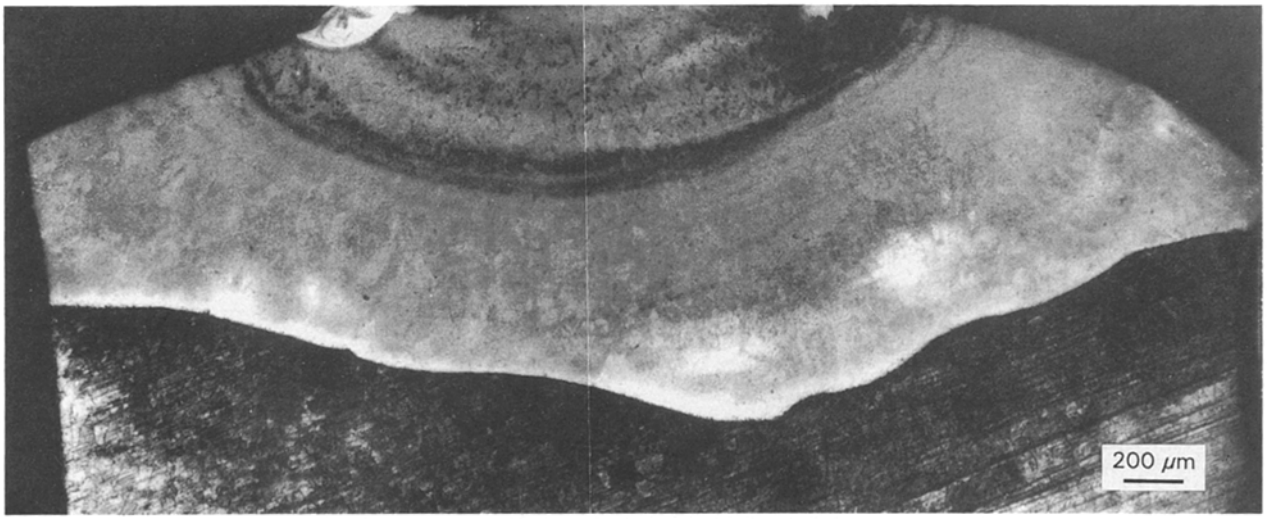

Figure 3 Optical micrograph of the laser-clad region (sample 2-1).

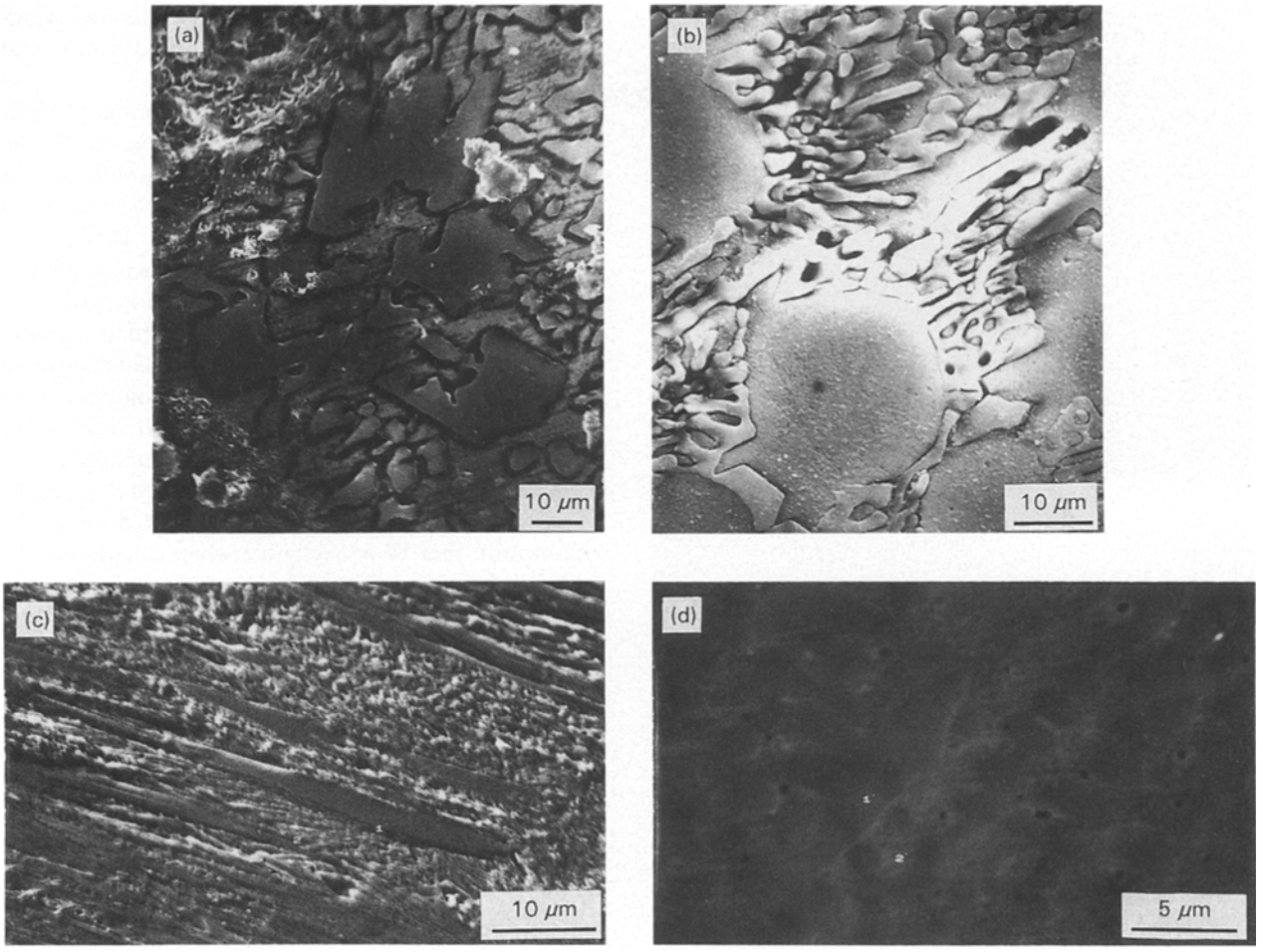

Figure 4 Carbide types from laser-clad Fe–Cr–C–W with preheated substrate: (a) diamond-shaped type (sample 7-2), (b) unfaceted-block diamond type (sample 1-1), (c) acicular type (sample 19-1), (d) cellular type (sample 8-2).

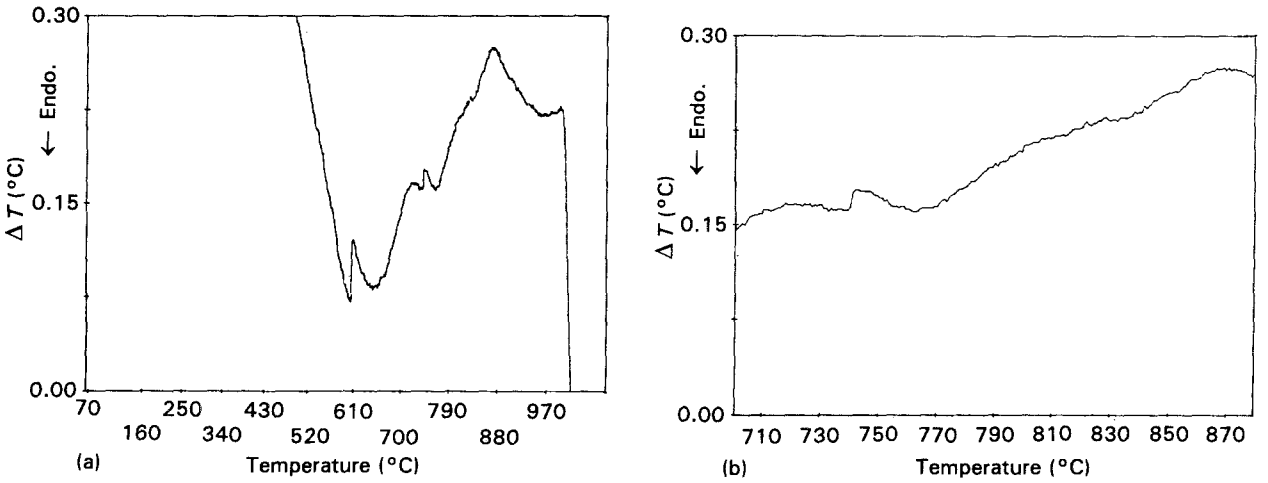

Figure 5(a, b) DTA results for sample without preheating: laser power 8 kW, beam diameter 3 mm, powder feed-rate 1.2075 gs^{-1}, traverse speed 1.693 cms^{-1}.

produced qualitatively. The results were listed qualitatively as shown in Table IV. This shows an SEM EDX qualitative analysis for sample 1-1. From a survey of the spectrum the relative height of the spectrum was calculated and a qualitative concentration obtained roughly. In fact, it was very hard to pick up the carbon spectrum line though EDX analysis because of the characteristics of SEM EDX, since EDX analysis uses the carbon spectrum line as one of the reference lines to detect the other spectrum lines.

Nevertheless, some idea of the metal element distribution in the carbides was obtained. Through this analysis it was deduced that blocked but unfaceted carbide was rich in Fe, while the phase between blocked but unfaceted carbides was comparatively rich in Cr. In particular the phase between the

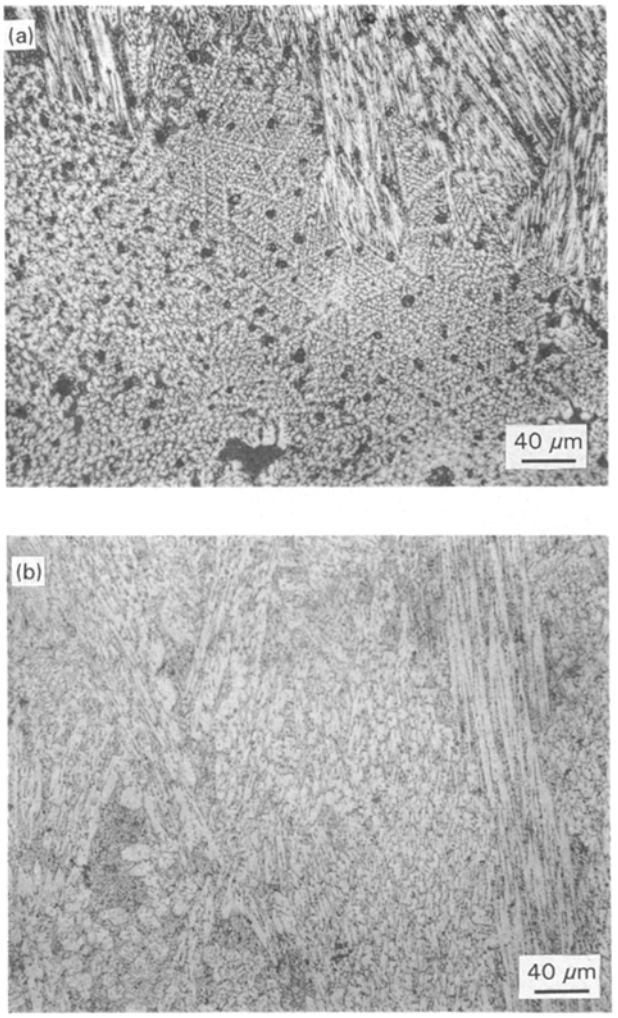

Figure 6 Comparison of microstructure (a) before and (b) after DTA for sample without preheating.

unfaceted-block carbides showed higher Cr and W concentrations than the unfaceted-block carbides. Fig. 7 shows the corresponding spectrum survey results, and Fig. 8 presents the corresponding SEM microstructure of sample 1-1.

3.1.4. Auger electron scanning analysis

In order to investigate the microchemistry of the clad region of the Fe–Cr–C–W semi-quantitatively, AES analysis was carried out. The blocked diamond-like carbide obtained from SEM microanalysis was examined to get the element atomic concentration and carbide compositions.

Table V with Figs 9–12 present a summary of the AES analysis for sample 19-1. Extracting the W element peak line from the AES survey was difficult due to the amount of W (1.6 at%) and the characteristics of the W element line in AES analysis. However, it could be assumed that the effect of W was negligible in the overall metal atomic concentration for prediction of carbide compositions because of its small amount. It was also found that point surveys to detect element compositions are affected by the sputtering time of the AES microscope as shown in Table V, due to the characteristics of AES analysis (surface analysis).

Many different carbides such as M_7C_3, M_6C, $M_{23}C_6$ as well as MC_2, MC were detected under the assumption that W is negligible when calculating the volume fraction of metal alloying concentration (Table V). In particular, more than 50% carbon concentration was observed at high-carbon areas in the AES C map (Table V points 5 and 6 of area 1, and Fig. 10). These regions contained just a small amount of Cr, while they were rich in iron. Thus, the carbide precipitates were assumed to have (Fe, Cr, W) C_2 type composition. Previous TEM analysis of the carbides from laser-clad Fe–Cr–W–C alloy without preheating also provided an indication of this possible structure [9, 17].

Diamond-shaped carbide precipitates, as shown in Fig. 10, were determined to be M_7C_3-type carbide. The diamond-shaped carbide precipitates were found to be rich in Fe element and also to have about 18–20 at % Cr (Table V points 1, 3 and 4 of area 1, and Fig. 10). Please note that these diamond shaped carbides look morphologically different than that reported in [2]. Carbides in this study lost the sharp edges evident in the previous study. This may be due to the preheating utilized in this study. Reduced cooling rate due to preheating seems to have also changed the composition from M_6C, as reported in [2], to M_7C_3.

Acicular-type carbide precipitates, as shown in Fig. 11, were also examined and concluded to be MC-type carbide. (Table V points 1 and 2 of area 2, and Fig. 11). Point surveys in between acicular-type carbides were

TABLE IV SEM EDX qualitative analysis (sample 1-1)

Position	Relative height of spectrum				Qualitative concentration (%)				Remarks
	Fe	Cr	W	C	Fe	Cr	W	C	
1	9.9	2.5	0.4	–	77.3	19.5	3.2	–	Blocked, non-faceted
2	> 13.4	10.2	11.9	0.25	–	–	–	–	Fine dendrite type
3	12.6	4.1	0.6	–	72.8	23.7	3.5	–	Blocked, non-faceted
4	10.7	33	0.37	–	76	21.3	2.7	–	Blocked, non-faceted
5	7.4	4.54	0.7	–	58.5	35.9	5.6	–	Fine dendrite type
6	10.5	2.9	0.4	–	76.1	21	2.9	–	Blocked, non-faceted
7	10.8	2.9	0.5	–	76.1	20.4	3.5	–	Blocked, non-faceted
8	5.35	6.15	0.75	–	43.7	50.2	6.1	–	Fine dendrite type
9	9.65	2.5	0.4	–	76.9	20	3.1	–	Blocked, non-faceted
10	6.15	5.1	0.75	–	51.2	42.5	6.3	–	Fine dendrite type
11	9.5	2.5	0.4	–	76.6	20.2	3.2	–	Blocked, non-faceted

also carried out and detected MC-type carbide precipitates. However, acicular-type carbides (Table V point 1 of area 2) were richer in Cr but lower in Fe, comparatively, but the area between acicular-type carbides (Table V point 2 of area 2) was found to be low in Cr and richer in Fe. The distribution of carbon in the clad region, as shown in Fig. 11, was uniform throughout the AES maps.

The same logic related to latest heat was brought to bear to understand the atomic concentration distributions of carbides associated with material processing parameters as reported by Li and Mazumder [16] and Singh and Mazumder [3]. Near the interface between clad alloy and substrate, the latent heat energy released during the cooling process plays a big role with respect to the substrate. This latent heat energy can not only melt an additional layer of the substrate but also affect the carbide concentration during solidification. Since the power density, an important overall processing parameter, alters the latent heat energy which affects the substrate, the amount of remixing layer and the carbide concentration in the clad can be affected by the latent heat energy. It is also shown that the additional effect of preheating could enhance the

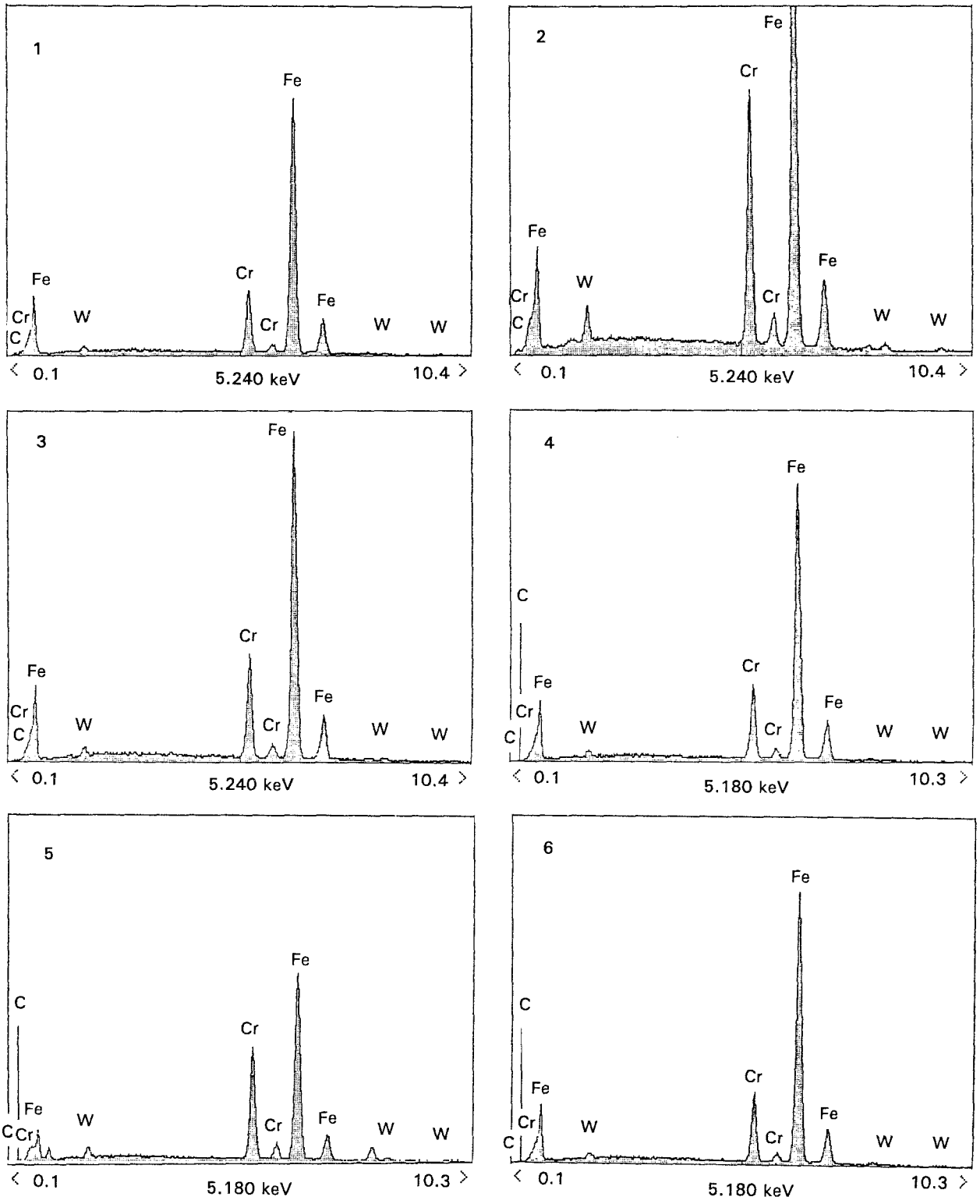

Figure 7 SEM EDX spectrum analyses for positions 1–11 at sample 1-1 (see Fig. 8 and Table IV).

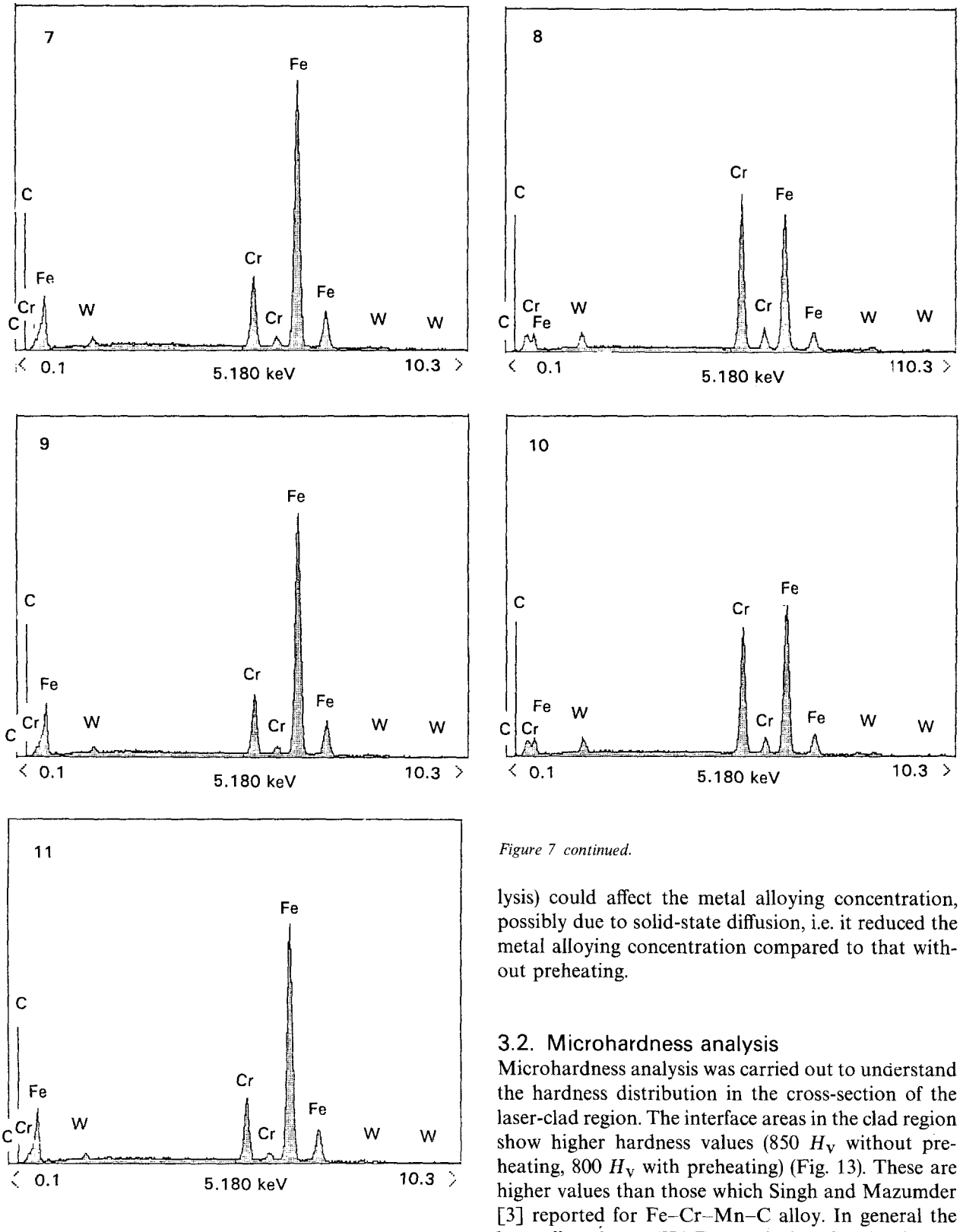

Figure 7 continued.

metal alloy concentration in the clad region with exposure for enough time to allow diffusion, especially above the phase transition temperature.

Since the carbide types are affected by power density as well as preheating temperature, one has to consider both effects to control the evolution of microstructure. It was observed that a higher power density leads to a higher alloying concentration of metal M near the interface and less in the middle of the clad, as long as there is no keyholing. However, it was also found that a preheating temperature above the phase transition (about 600 °C in this case from DTA analysis) could affect the metal alloying concentration, possibly due to solid-state diffusion, i.e. it reduced the metal alloying concentration compared to that without preheating.

3.2. Microhardness analysis

Microhardness analysis was carried out to understand the hardness distribution in the cross-section of the laser-clad region. The interface areas in the clad region show higher hardness values (850 H_V without preheating, 800 H_V with preheating) (Fig. 13). These are higher values than those which Singh and Mazumder [3] reported for Fe–Cr–Mn–C alloy. In general the heat-affected zone (HAZ) near the interface has higher hardness values than in the lower substrate, due to the finer grain sizes resulting from the higher cooling rate associated with transformation of the microstructures. Fig. 13 shows the hardness distribution for a sample which was not preheated. No significant drop of hardness was found through comparing the preheated with the non-preheated samples.

The hardness distribution in terms of preheating temperature (Fig. 14) was plotted to understand the role of preheating temperature in hardness distribution. Although it is difficult to deduce the role of preheating temperature, it was observed that the

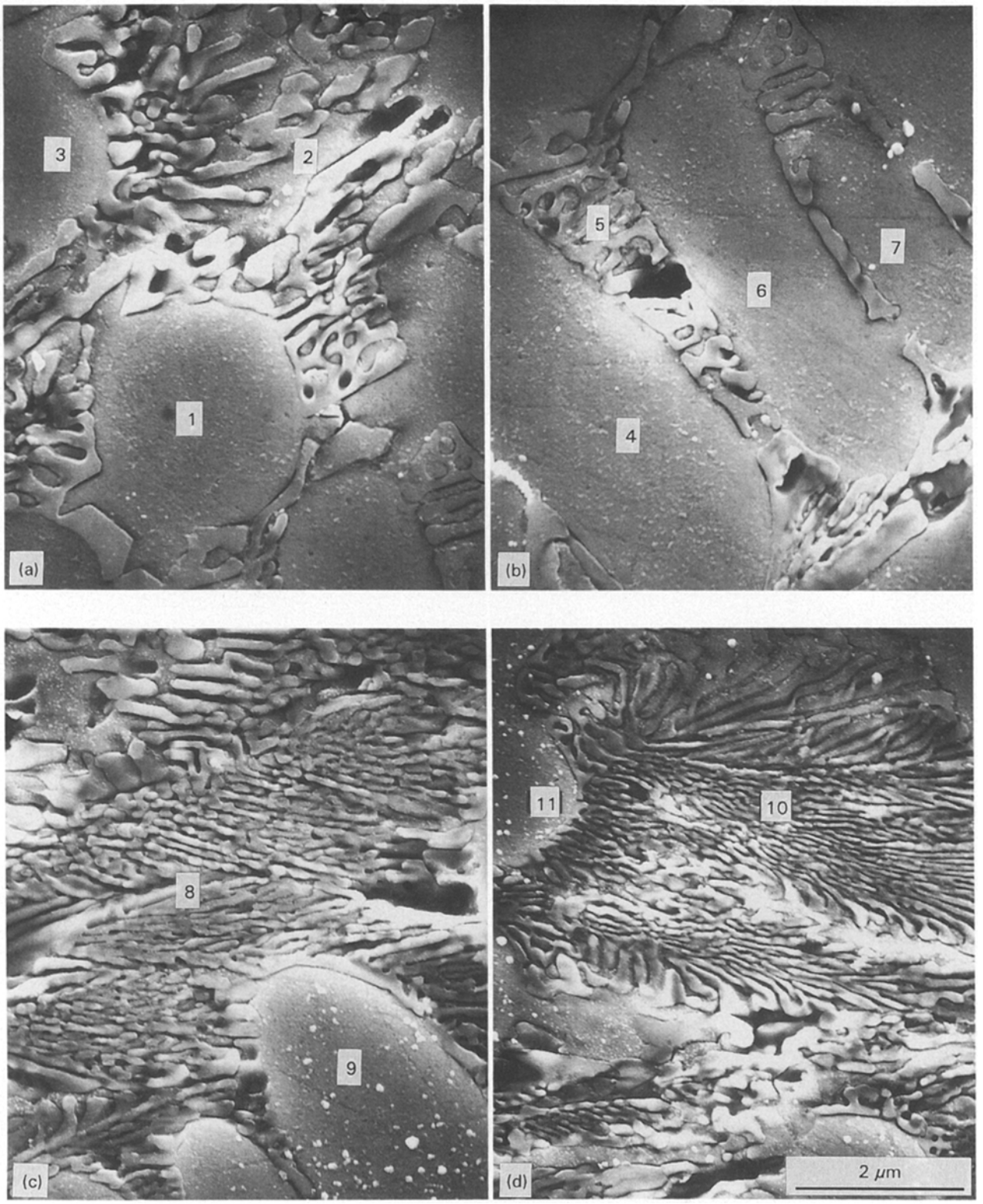

Figure 8 SEM micrograph of sample 1-1.

preheating temperature could affect the hardness distribution considerably compared to the samples without preheating. Due to lack of metallurgical information, exact results concerning the role of preheating temperature could not be obtained, but detailed analysis will be carried out and reported in the near future.

The hardness distribution as a function of power density (Fig. 15) was obtained to understand the influence of the overall laser processing parameter. The results show that the average hardness increases as the power density increases; this is explained by the fact that, based on the laser cladding mechanism [16], a higher power density will lead to a lower cooling rate which in turn produces a larger carbide grain size. Thus the large carbide precipitates will affect the carbide distribution in the matrix to give a higher hardness value. In addition to this carbide size effect, the dissolution of W in the carbide precipitates could contribute to enriching the metal concentration of

TABLE V Summary of AES analysis (sample 19–1)[a]

Area No.	Point No.	Element concentration (%)[b]				Compositions of positions			Sputter time (min)	Description of point in area
		C_1	O_1	Cr_2	Fe_3	Metal (%)	Carbon (%)	Carbide type[c]		
1	1	25.10	27.62	18.17	29.12	65.3	34.7	M_7C_3	5	Dark, blocked
	2	9.89	24.96	5.61	59.54	86.8	13.2	M_6C	5	Light, smooth
	1	13.34	33.09	9.80	43.77	80	20	$M_{23}C_6$	40	Dark, blocked
	2	15.71	27.36	4.98	51.95	78.4	21.6	$M_{23}C_6$	40	Light, smooth
	3	20.86	30.62	17.75	30.77	69.9	30.1	M_7C_3	40	Dark, blocked
	4	19.86	30.12	19.25	30.81	71.6	28.4	M_7C_3	40	Dark, blocked
	5	54.52	19.86	0.94	24.67	32	68	MC_2	40	High carbon area after C map
	6	52.86	23.08	5.75	18.31	31.3	68.7	MC_2	40	High carbon area after C map
2	1	52.77	8.20	18.78	20.25	43	57	MC	40	Acicular type carbide
	2	46.55	6.99	8.25	38.20	50	50	MC	40	Point between acicular carbides

[a] Fe–Cr–C–W (10:4:1:1 wt%, 51.9:22.3:24.2:1.6 at%).
[b] The tungsten peak is hard to detect.
[c] Carbon/metal percentages as follows: M_3C 25/75, M_6C 14.3/85.7, M_7C_3 30/70, $M_{23}C_6$ 20.7/79.3.

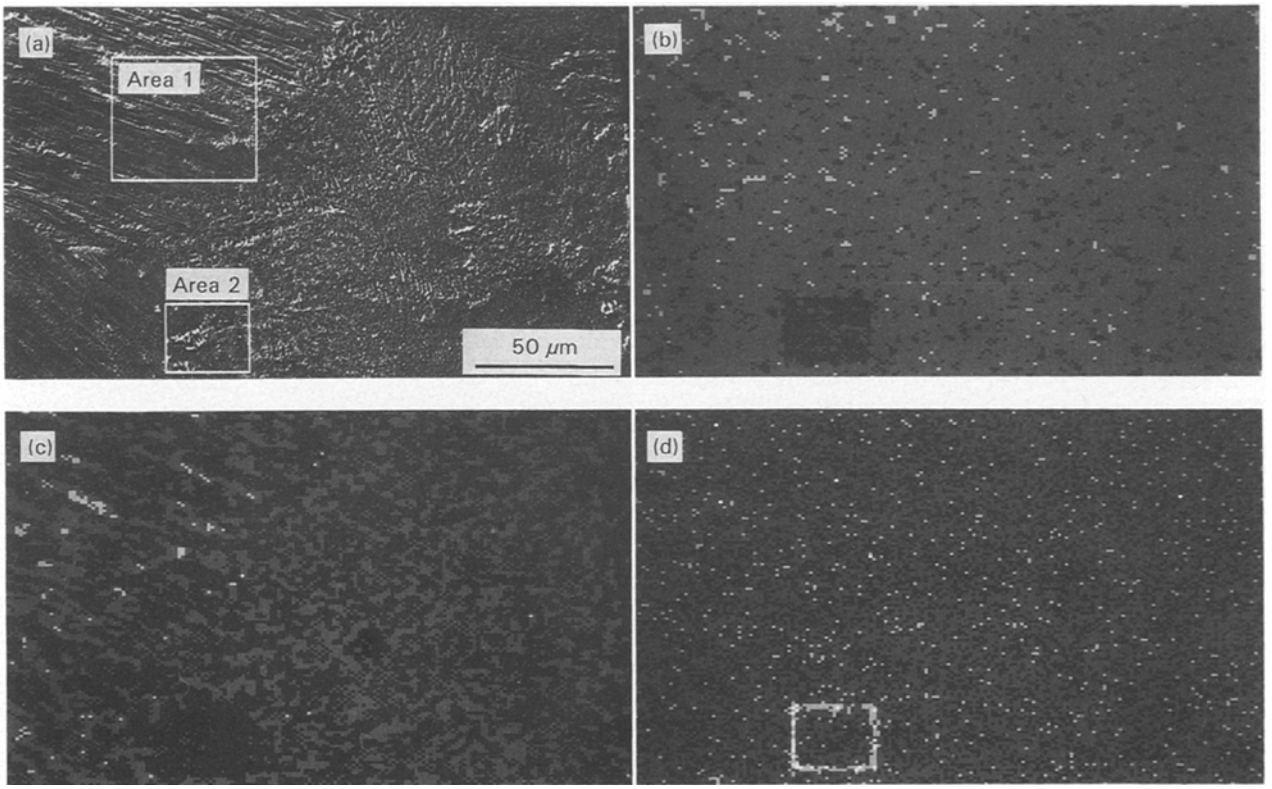

Figure 9 (a) SEM micrograph of sample 19-1, and AES maps for (b) Fe, (c) Cr and (d) C.

carbides, because the W concentration is enhanced as the power density increases. Also, the hardness near the interface generally shows a higher value than the average hardness of the entire cladding area, as already observed and explained from the cladding mechanism based on heat and mass transfer during the interaction.

3.3. Wear analysis

Wear tests were carried out to study the tribological characteristics for laser-clad Fe–Cr–C–W alloys. A data set for this wear test is provided in Table VI. The widths of the wear scars obtained from wear tests give a relative measurement of the wear resistance. The range of average wear scar was generally between 0.30 and 0.55 mm after a 1 h run. These data show better wear properties than the data for Fe–Cr–Mn–C laser cladding already obtained by Singh and Mazumder [3] and Eiholzer *et al.* [1]. Fig. 16 shows a typical wear scar. The scar width was found to depend upon laser processing parameters such as power density, as shown in Fig. 17.

Fig. 17 shows the friction and wear of a laser-clad surface as a function of power density. The wear scar, generally associated with the friction coefficient, is

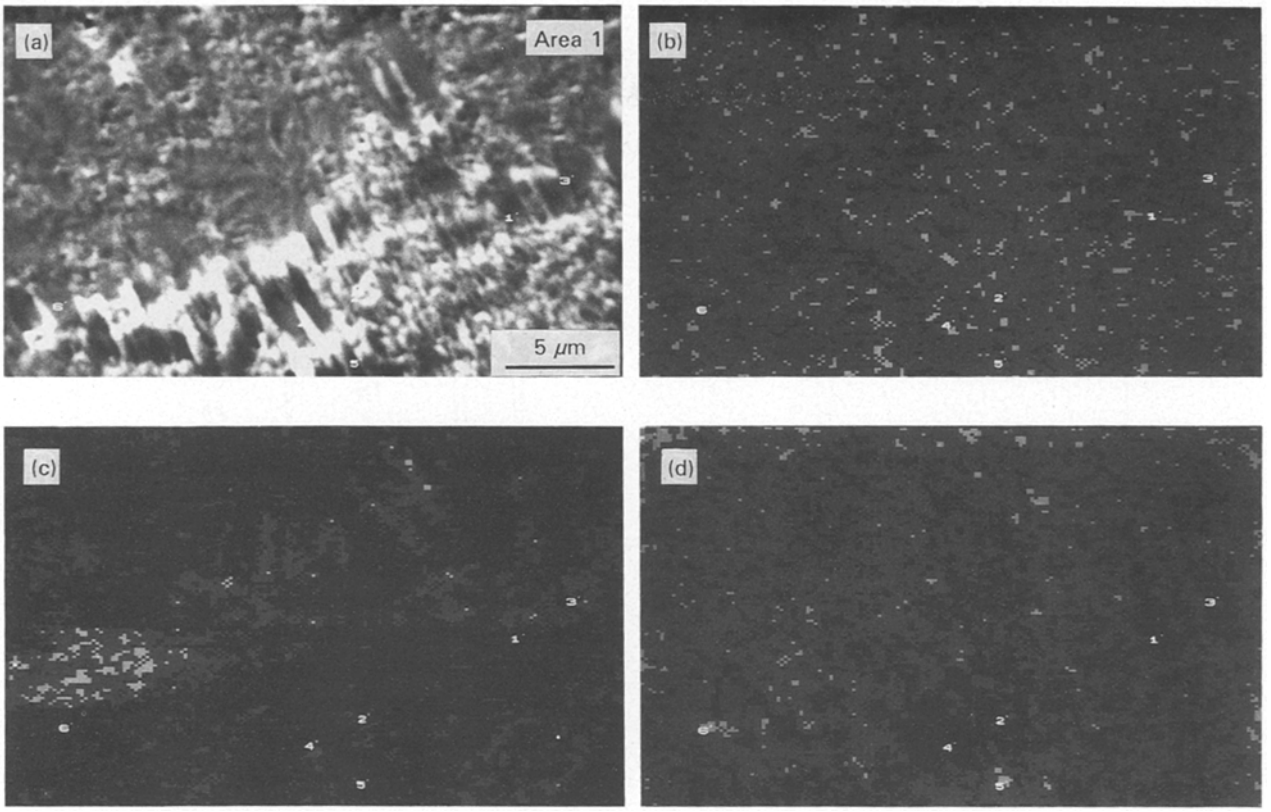

Figure 10 (a) SEM micrograph of area 1 of Fig. 9, and AES maps for (b) Fe, (c) Cr and (d) C.

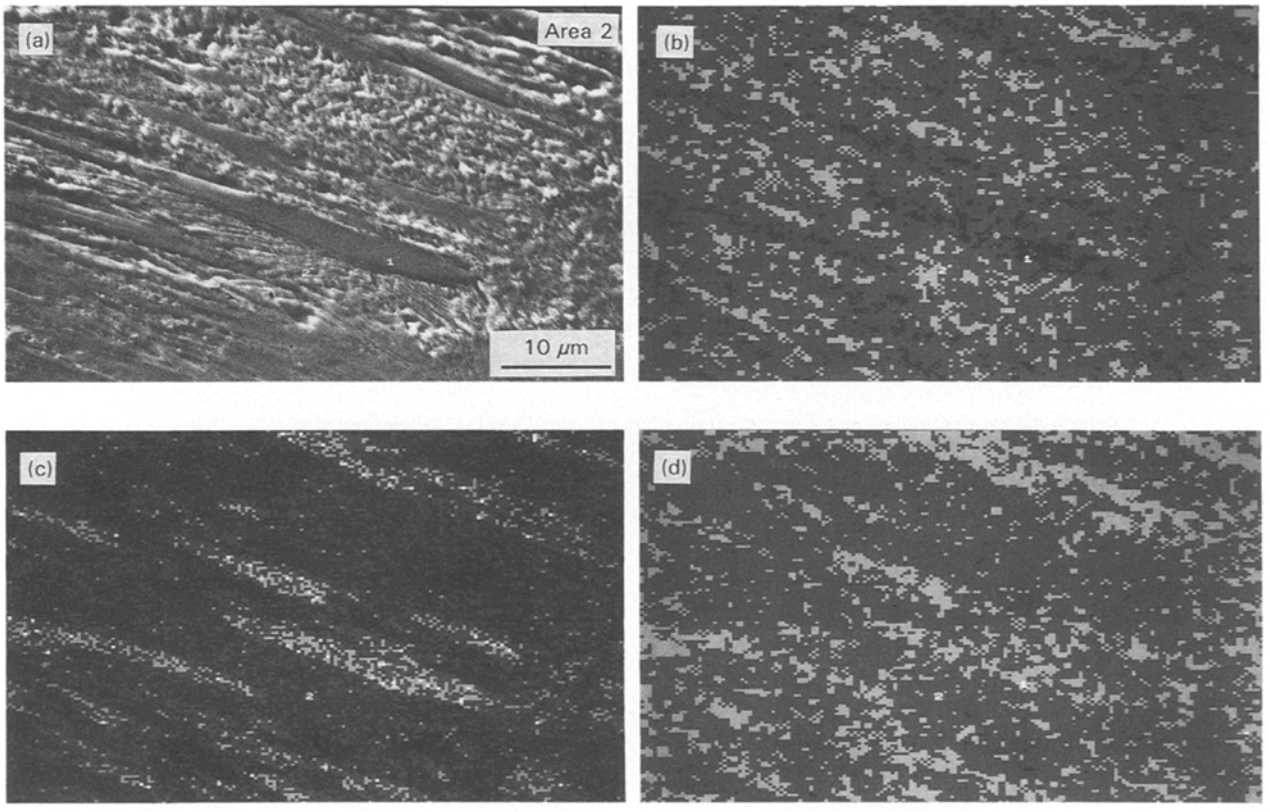

Figure 11 (a) SEM micrograph of area 2 of Fig. 9, and AES maps for (b) Fe, (c) Cr and (d) C.

observed to be dependent on power density as well as specific energy, and both are overall laser processing parameters. This can be explained by saying that a lower power density or lower specific energy input brings a higher cooling rate which, in turn, produces a finer microstructure with better wear [16]. This tendency, that a low power density is better for wear characteristics, must be opposite to the tendency in the hardness that a high power density leads to a relatively high hardness distribution, already described in previous results. Thus, one might control the laser processing parameters to have the proper

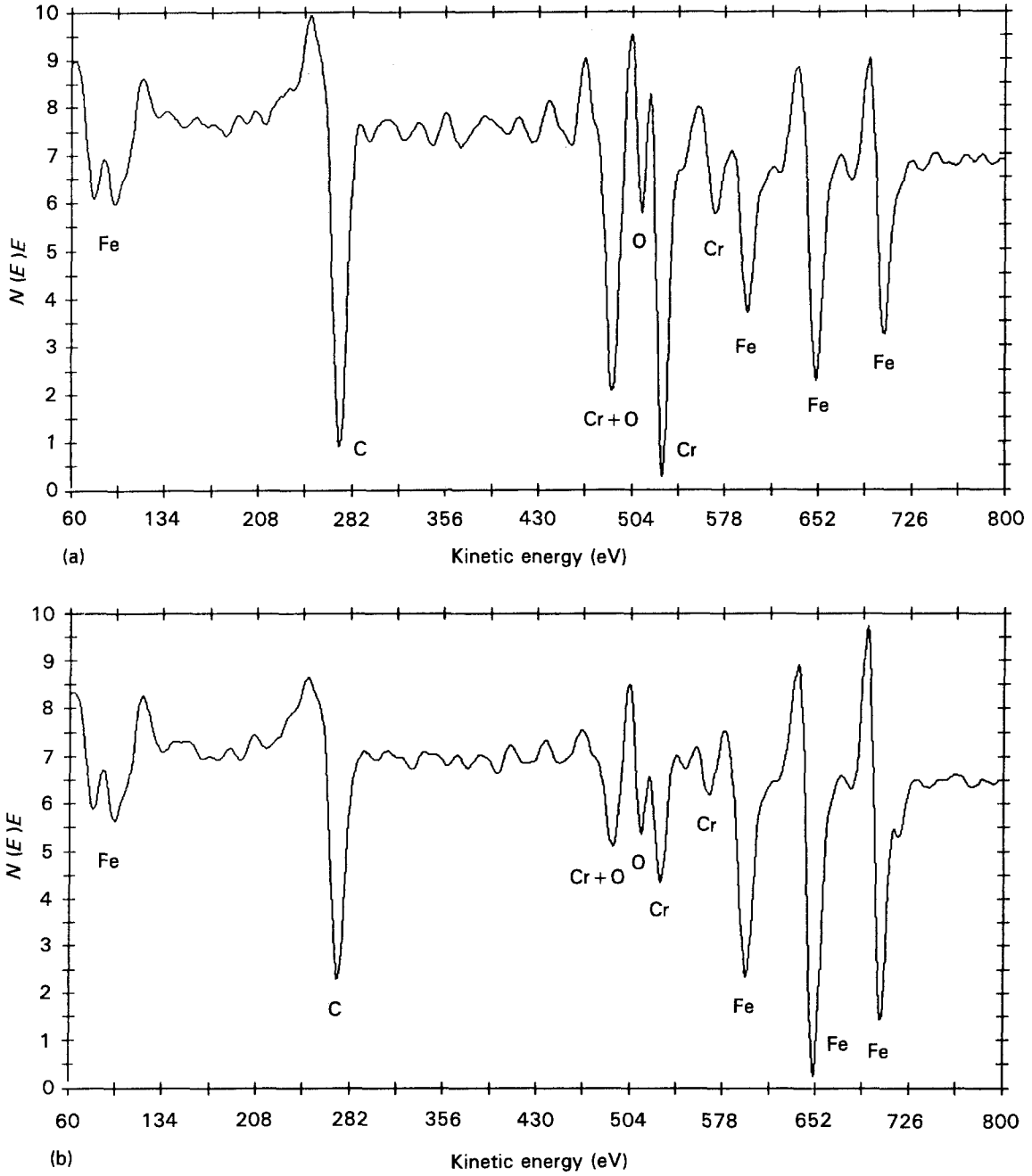

Figure 12 AES multiprobe surveys from (a) area 1 of Fig. 9 (Fig. 10 point 2, on elongated carbide) and (b) area 2 of Fig. 9 (Fig. 11 point 2, between carbides).

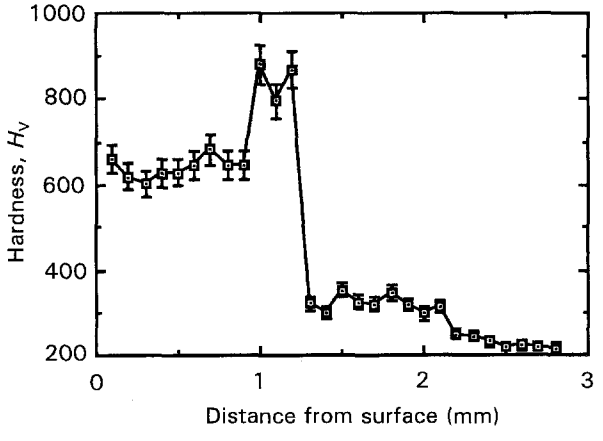

Figure 13 Hardness distribution as a function of distance from the top for sample without preheating.

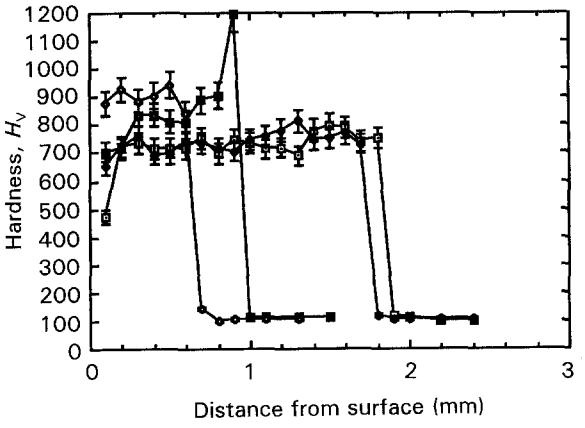

Figure 14 Effect of preheating temperature on hardness distribution: laser power 4 kW, beam dia. 4 mm, traverse speed 635 mm min^{-1}, powder feed-rate 0.5368 $g\,s^{-1}$. T = (◇) 298 °C, (◆) 400 °C, (□) 663 °C, (⊡) 725 °C.

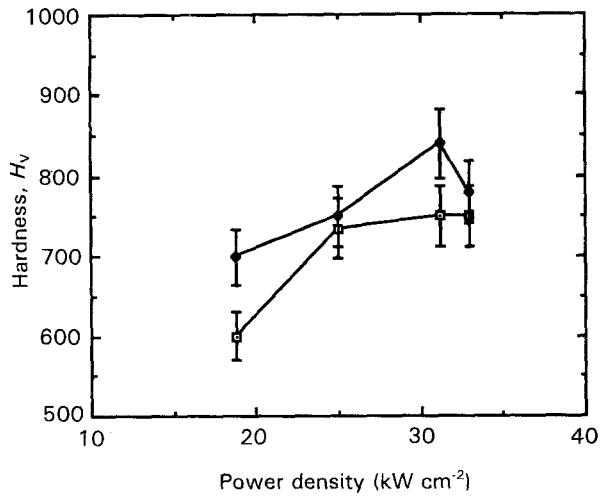

Figure 15 Hardness distribution as a function of power density: (⊡) average, (◆) interface.

clad which is desired in a certain situation. However, this may not be easy but needs optimization of the processing conditions to satisfy both hardness and wear requirements.

The friction coefficient as a function of sliding distance was also investigated as shown Fig. 18, from which it could be observed that the friction coefficient is high initially and is stable after reaching a certain sliding distance. The friction coefficient was also fairly low, which is desirable. This might be attributed to the fact that the test was done under lubrication. The steady-state friction coefficient, although there is a limiting value, tends to reduce as the laser power decreases, which means that the friction coefficient could also be controlled by the laser material processing parameters.

It seems that the overall wear properties of laser-clad Fe–Cr–C–W show better tribological characteristics to give enough advantages to replace conventional alloys, as already indicated in the paper of Eiholzer *et al.* [1].

4. Discussion

The first step to improve the laser-clad Fe–Cr–C–W alloy was the elimination of cracks in the clad during the laser-cladding process. The main reason for cracking seemed to be the extremely high temperature difference between the melting pool, which exists in the alloying state (Fe, Cr, C, W) at high temperature, and the substrate at room temperature. During the solidification process the interface with the clad would be solidified first, i.e. the solidification front would be in the interface due to melting-point differences between alloying elements and substrate as well as the huge temperature difference. This extreme temperature gradient causes considerable amounts of thermal stress, and then leads to cracks during the cooling process. In order to avoid these undesirable cracks a preheating process was selected because it could reduce the high temperature gradient which results in high thermal stresses. Thus the use of a preheated substrate before laser irradiation would eliminate the tensile solidification stresses; however, the preheating temperature could also lessen the advantage of laser processing, as it could reduce the extreme temperature gradient which leads to a non-equilibrium process. Nevertheless there would exist certain temperature ranges to obtain a crack-free clad without any significant losses of the advantages of the laser cladding process. In this research it was found satisfactory to obtain a crack-free clad in the temperature range 550–600 °C. This range could also be changed through the processing conditions or alloying composition.

The laser processing parameters affect the clad properties. In terms of microstructures in the laser cladding area, laser power density, which is an overall processing parameter, could control the size of carbides. It was observed that the carbide size increases with increase of laser power density. The microhardness measurement revealed that increasing laser power density leads to an increase in hardness because large carbides, which affect the hardness values, would be dominant and their distribution density would be increased due to the high laser power density. In contrast, the width of wear scar, which is one of the characteristic wear parameters, was found to increase with increasing laser power density. The friction coefficient also showed the same characteristics as the wear scar. Thus it would be recommended that a lower laser power density has advantages in terms of wear scar and friction coefficient because it brings a distribution of smaller carbides in the matrix phase, and thus less wear scar and a lower friction coefficient, as already mentioned in the previous section.

It has been observed that higher power density leads to higher average hardness, as already shown in Fig. 15, while lower power density or lower specific

TABLE VI Sample data set for wear test

Sample No.	Laser power (kW)	Beam dia. (mm)	Traverse speed (mm s^{-1})	Powder feed-rate (g s^{-1})	Preheat temperature (°C)	Specific energy (10^4 J cm^{-2})	Power density (10^4 W cm^{-2})	Wear scar (mm)	Friction coefficient
1-1	3	4	9.31	0.5368	600	0.805	1.875	0.3	0.1
2-1	5	4	11.85	0.5368	612	1.0546	3.125	0.45	0.113
7-2	4	4	10.58	0.5368	698	0.94475	2.5	0.35	0.114
8-2	4	3	11.85	0.5368	700	1.1248	4.44	0.55	0.112
13-1	3	3	11.43	0.5368	426	0.86625	3.3	0.35	0.109
16-1	4	4	10.58	0.5368	298	0.94475	2.5	0.35	0.11
19-3	4	4	11.01	0.5368	513	0.9085	2.5	0.4	0.111

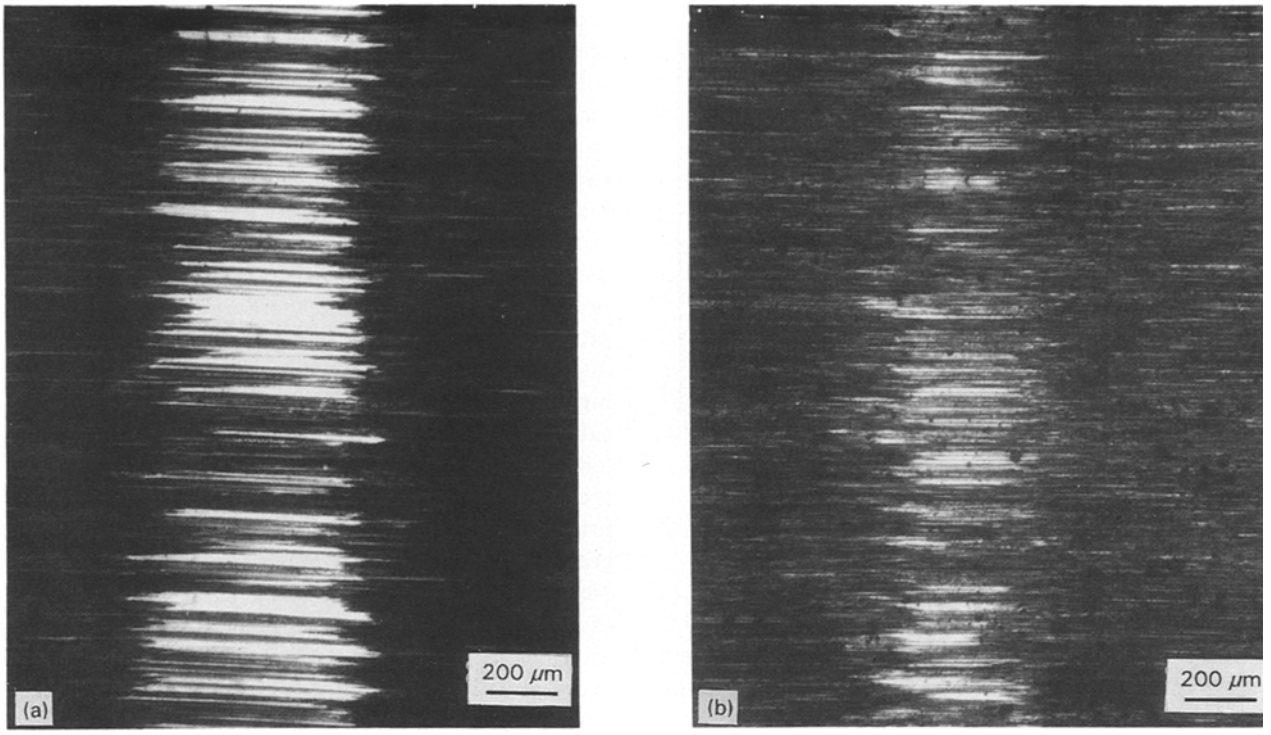

Figure 16 Typical wear scars after 1 h runs: (a) sample 8-2, (b) sample 7-2.

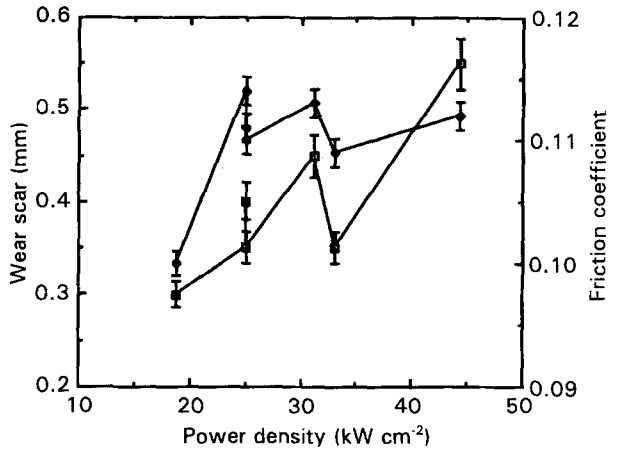

Figure 17 (◆) Friction coefficient and (⊡) wear scar of laser-clad surface as a function of power density.

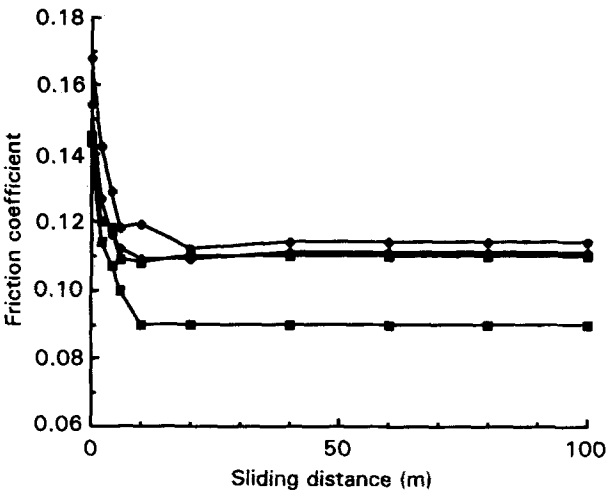

Figure 18 Friction coefficient as a function of sliding distance (beam dia. 4 mm, powder feed-rate 0.5368 g s^{-1}, traverse speed 635 mm min^{-1}): (⊡) sample 1-1 (laser power 3 kW), (◆) sample 2-1 (laser power 5 kW), (■) sample 16-1 (laser power 4 kW), (◇) sample 19-3 (laser power 4 kW).

energy produces better wear properties, with a smaller wear scar, as shown in Fig. 17. Thus it may be questioned which processing parameters are reasonable to get the synthesis of Fe–Cr–C–W with good microhardness and tribological characteristics. One worker may choose lower power density values but another may choose somewhat higher values although the difference of power density level is not so large. There would be optimal ranges to get a desirable laser clad. Nevertheless, it may not be easy to find the proper processing conditions at one time, because the laser cladding process is an entirely non-equilibrium process. Therefore, in order to get successful cladding results, it should be understood that carbide formation, the key factor to affect the properties in this research, is closely associated with laser processing parameters as well as cooling temperature. In addition one should check the effects of preheating during the process, because it sometimes gives abnormal conditions which are undesirable when not well controlled. However, one might determine process parameters based on the trade-off between hardness and wear.

The general microstructural survey of the laser cladding area shows very different and complex types of carbide which depend upon the laser processing conditions such as laser power and beam diameter, as well as the preheating temperature. Another important thing from the metallurgical point of view is the concentration or volume fraction of the carbides. In order to summarize the metallurgical characteristics of this alloy, a knowledge of the carbide formation is imperative. In general, carbide types were various as a function of the process parameters because of the

nature of this non-equilibrium process. It was concluded from the SEM and AES analyses that the formation of carbides should be considered with regard to both laser processing conditions and cooling rate or preheating temperature in this case.

Both diamond-shaped carbides and acicular-type carbides were found to show good characteristics in terms of both the hardness distribution and the wear resistance. They also indicated a high metal volume fraction which could form the M_6C or $M_{23}C_6$ type of carbide observed in the metallographical analyses (SEM and AES). On the other hand, unfaceted-block carbides were observed to contain a high carbon concentration which could form the M_2C_3 or M_2C_5 type carbides. It could be expected that the dissolution time for metal elements such as Cr or W, which could enhance the carbide concentration and give a better hardness distribution and wear resistance, could be used to control the carbide formation. Matrix phases, which are relatively lower in alloy concentration, could be soft enough to offer a damping effect. The dissolution time could be controlled by the traverse speed, also a laser processing parameter. If optimal power density and traverse speed are used, the metal elements have sufficient time to dissolve in the form of carbide precipitates which are rich in metals, in addition getting a good wear resistance and adequate hardness distribution.

Fig. 19 suggests that by controlling laser process parameters, for instance, power density or specific energy, the solid solubility of the metal elements in the matrix as well as the carbides could be manipulated. It was constructed on the basis of microstructure analysis results (AES and SEM EDX). The same kind of observation was made for Fe–Cr–Mn–C alloy [3].

Clad thickness and width also can be determined by controlling laser processing parameters such as beam diameter. For instance, it can be clearly proved that a 4 mm beam diameter gives a lower clad thickness than 3 mm, i.e. the clad thickness can be controlled by material processing parameters.

As a result, one should understand the importance of laser processing parameters which significantly affect the microstructure as well as the microchemistry of the clad in order to obtain good wear properties with a desirable hardness distribution. However, it may require careful experimentation to yield the optimal combination of processing parameters.

5. Summary and conclusions

The effects of process parameters and preheating temperature on the microstructure and properties of laser-clad Fe–Cr–W–C alloys are discussed. The most important conclusions from this study are as follows:

1. Control of the cooling rate by preheating is essential to form a crack-free clad for such alloys with a high concentration of carbides.
2. The composition and volume fraction of carbides can be controlled by controlling the preheating temperature, power density and traverse speed.
3. Diamond-shaped M_6C-type carbide seems to promote better wear resistance. However, many types of carbide such as M_7C_3, $M_{23}C_6$, MC_2 and MC are observed.
4. Higher power density leads to large carbide precipitates, resulting in high hardness but relatively lower wear resistance.
5. Lower power density leads to finer carbide precipitate, resulting in better wear resistance.
6. Carbides near the interface are generally metal-rich.
7. Selection of optimum process parameters is necessary to obtain a trade-off between wear and hardness.

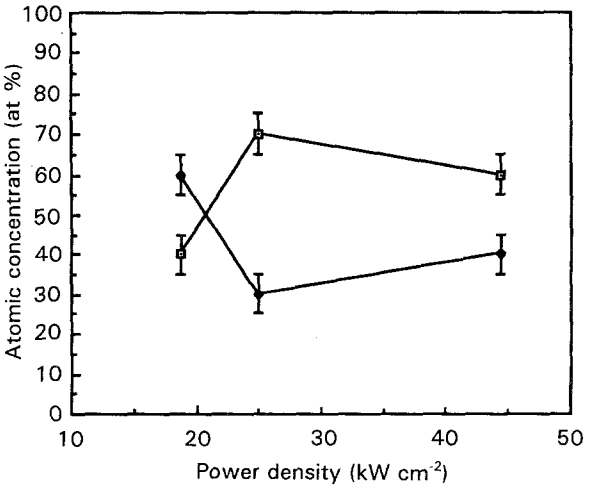

Figure 19 Atomic concentration of carbide as a function of power density: (⊡) concentration of metal alloying, (◆) concentration of carbon.

As earlier studies have indicated, these laser-clad Fe–Cr–C–X (X = W, Mn, etc.) exhibit superior wear properties to cobalt-bearing Stellite alloys and offer a possibility for conservation of strategic materials [3, 17].

Acknowledgement

This work was partly made possible by support from Daewoo Heavy Industries Ltd in Korea. The initial work on laser-clad Fe–Cr–W–C alloys was funded by Quantum Laser Corporation. The studies involving electron microscopy were performed in the Center for Microanalysis of Materials in the Materials Research Laboratory of the University of Illinois at Urbana–Champaign. The wear tests were carried out with the help of Professor C. Cusano at the Mechanical and Industrial Engineering Department at the University of Illinois at Urbana–Champaign.

References

1. E. EIHOLZER, C. CUSANO and J. MAZUMDER, in Proceedings of International Congress on Application of Lasers and Electro-Optics, Boston, Massachusetts, edited by J. Mazumder, *Materials Processing* Vol. 44 (Laser Institute of America, 1984) p. 159.
2. J. SINGH and J. MAZUMDER, *J. Mater. Sci. Tech.* **2** (1986) 709.

3. *Idem, Met. Trans.* **18A** (1987) 313.
4. H. L. GOLDSCHMIDT, *J. Iron Steel Inst.* **170** (1952) 189.
5. B. UHRENIUS and S. FRONDELL, *Met. Sci.* **11** (1977) 73.
6. M. BERGSTÖM, *Mater. Sci. Eng.* **27** (1977) 271.
7. *Idem, ibid.* **27** (1977) 257.
8. P. GUSTAFSON, *Met. Trans.* **19A**, (1988) 2547.
9. J. SINGH and J. MAZUMDER, unpublished report at University of Illinois at Urbana–Champaign (1988).
10. J. D. AYERS, T. R. TUCKER and R. J. SCHAEFER, in Proceedings of the Second International Conference on Rapid Processing, Restron, VA, March 23–26, 1980, edited by R. Mehrabias, H. H. Kear and M. Cohen (Claitor's Publishing Division, 1980) pp 212–220.
11. V. M. WEERASINGHE and W. M. STEEN, in Proceedings of Conference on Lasers in Material Processing, Los Angeles edited by E. Metzbower (ASM International, Ohio, 1983), pp. 166–175.
12. J. SINGH and J. MAZUMDER, *Acta. Metall.* **8** (1987) 1995.
13. A. BELMONDO and M. CASTAGNA, *Thin Solid Films* **64** (1979) 249–256.
14. N. A. GLAESER and B. P. FAIRAND, in "Wear of Materials", International Conference on Wear of Materials, Dearborn, MI, edited by K. C. Ludema, N. A. Glaeser, and S. K. Rhez (ASME, 1979).
15. J. MAZUMDER and J. SINGH, US Patent Application, 133 346 (1987).
16. L. J. LI and J. MAZUMDER, in Proceedings of Conference on Laser Processing of Materials, Los Angeles, CA, February 26–March 1, 1984, edited by K. Mukherjee and J. Mazumder (TMS-AIME, Warrendale, Pennsylvania, 1984) pp. 35–50.
17. J. MAZUMDER, J. CHOI, C. RIBAUDO, A. WANG and A. KAR, in Proceedings of Internationl Conference on Beam Processing of Advanced Materials, Chicago, IL, November 2–5, 1993, edited by J. Singh and S. M. Copley, (TMS-AIME, Warrendale, Pennsylvania, 1993) p. 41.

Received 16 August
and accepted 14 September 1993